

RESEARCH ARTICLE OPEN ACCESS

Designer Glycolysomes: Colocalisation of Glycolytic Enzymes on a Cellulosome-Based Synthetic Protein Scaffold

Marte Elias^{1,2}  | Kenan Meert^{1,3,4}  | Julie Vanderstraeten¹  | Babette Lamote^{1,2}  | Yves Briens¹ 

¹Department of Biotechnology, Laboratory of Applied Biotechnology, Ghent University, Ghent, Belgium | ²Department of Biotechnology, Center for Synthetic Biology, Ghent University, Ghent, Belgium | ³Department of Plants and Crops, Laboratory of Applied Mycology and Phenomics, Ghent University, Ghent, Belgium | ⁴Biotalys NV, Ghent, Belgium

Correspondence: Yves Briens (yves.briens@ugent.be)

Received: 14 November 2024 | **Revised:** 27 February 2025 | **Accepted:** 5 March 2025

Funding: This work was supported by Bijzonder Onderzoeksfonds UGent, (BOF16/STA/024, BOF17/DOC/086), Research Foundation—Flanders (FWO) (1S20622N, 1S20624N, 1SE2623N), and Flanders Innovation and Entrepreneurship (HBC.2023.0138).

Keywords: biocatalysis | enzyme cascade | enzyme colocalization | enzyme scaffold | glycolysis | pathway efficiency | system biocatalysis

ABSTRACT

In systems biocatalysis, combining pathway enzymes *in vitro* allows for the conversion of basic substrates into more complex, valuable chemicals. However, *in vitro* enzyme cascades are not yet economically viable for large-scale bio-based chemical production. Enhancing pathway efficiency through enzyme colocalization on synthetic protein scaffolds is a proposed solution, though still debated. We constructed a synthetic protein scaffold that colocalises the first three glycolytic enzymes using cohesin–dockerin interactions. Initially, we converted wild-type enzymes to the docking enzyme mode and evaluated their activity. Next, we demonstrate how the colocalisation of the three docking enzymes on distinct scaffolds enhances the enzyme cascade's production. Starting from glucose, the multi-enzyme complexes produced fructose-1,6-bisphosphate, confirming the activity of each enzyme. PfkA, which converts fructose-6-phosphate and ATP to fructose-1,6-bisphosphate and ADP, was identified as the rate-limiting enzyme. We demonstrated that scaffolding proximity effects lead to higher product output than free docking enzymes, particularly at lower enzyme densities. Further research is needed to determine the relevance of enzyme colocalisation under industrial production settings. In addition, optimising an enzyme cascade demands a thorough understanding of reaction mechanisms and kinetics. The VersaTile method streamlines optimisation studies of modular proteins and complexes, enabling analysis of a broader design space by bypassing technical preparatory hurdles.

1 | Introduction

Glucose occupies a central position in the metabolism of all living cells. It is the most abundant monosaccharide in nature and has a high energy potential ($\Delta G^{\circ} = -686$ kcal/mol), making it a good cellular fuel (Cooper 2000). Moreover, glucose is a remarkably adaptable precursor, capable of supplying an array of intermediates for biosynthetic reactions. For example, *Escherichia coli* obtains all necessary building blocks for the production of

each amino acid, nucleotide, coenzyme, fatty acid and other intermediates it needs for growth from glucose. The synthesis of these primary metabolites occurs via a range of consecutive metabolic pathways (Wang and Yan 2018).

The first and central metabolic pathway is glycolysis (Embden–Meyerhof–Parnas pathway). Here, glucose is converted to pyruvate in a series of ten enzyme-catalysed reactions. The first five reactions constitute the preparatory phase. Here, glucose

Marte Elias and Kenan Meert contributed equally to this study.

This is an open access article under the terms of the [Creative Commons Attribution-NonCommercial](https://creativecommons.org/licenses/by-nc/4.0/) License, which permits use, distribution and reproduction in any medium, provided the original work is properly cited and is not used for commercial purposes.

© 2025 The Author(s). *Microbial Biotechnology* published by John Wiley & Sons Ltd.

is converted into two molecules of glyceraldehyde-3-phosphate (G3P) by the use of two ATP molecules. Both G3P molecules then enter the pay-off phase, where each is converted into pyruvate, producing a total of four ATP and two NADH molecules (Nelson and Cox 2013). This results in a net energy gain of two ATP molecules. Although glycolysis is usually described as a cytosolic process, literature describes that several organisms tend to colocalize their glycolytic enzymes. For example, trypanosomatids sequester glycolytic enzymes inside specialised organelles called glycosomes (Haanstra et al. 2014). In the case of *Caenorhabditis elegans*, glycolytic enzymes compartmentalise near synapses under conditions of energy stress. As such, high local levels of ATP can be maintained (Jang et al. 2016). In *Saccharomyces cerevisiae*, a glycolytic metabolon appears to associate with the cytoskeleton (Araiza-Olivera et al. 2013). In *Arabidopsis* cells, the glycolytic enzymes were found to be functionally associated with the mitochondrion (Giegé et al. 2003). The authors proposed that this compartmentalization enables direct delivery of pyruvate to the mitochondrion, where it serves as a respiratory substrate for the citric acid cycle.

The glycolytic starting point, glucose, is a cheap and renewable substrate. However, it should be noted that the sustainability of glucose depends on its source: glucose derived from starch-based food sources can increase pressure on food prices, while glucose from cellulosic materials is more sustainable but requires additional processing. In contrast, several glycolytic intermediates are expensive and can serve as starter materials for the production of a large range of fine chemicals, explaining the general interest in applying glycolytic enzymes in industrial processes (Deng et al. 2005; Jain et al. 2016; Li et al. 2012; Moon et al. 2009; Sze et al. 2016; Wang and Yan 2018). In metabolic engineering, researchers aim to boost metabolic flux to increase the production of a specific chemical. A potential approach is to target the glycolytic pathway through the engineering of industrial microorganisms. However, as a primary metabolic pathway, glycolysis is tightly regulated (Wang and Yan 2018). As a result, many attempts to enhance glycolytic flux, by over-expressing homologous or heterologous genes encoding glycolytic enzymes, have been unsuccessful (Jojima and Inui 2015). Additionally, in vivo cell-based fermentations often face drawbacks such as competition with the central cellular metabolism and the challenge of predicting regulatory network interactions (Ullah et al. 2016). A possible solution to circumvent these problems is systems biocatalysis, where engineered enzymes are used in vitro for the production of a desired fine chemical. An in vitro glycolysis was successfully reconstructed from ten purified *E. coli* enzymes by Itoh et al. (2004) and Stevenson et al. (2012). In the case of Stevenson and colleagues, the composition of each enzyme was initially set according to the reported activities. Later, different enzyme ratios were tested. The most critical ratio was Glk:PfkA, which was found to be optimal at 1:50. In a study by Itoh et al. (2004), capillary electrophoresis-mass spectrometry allowed for direct, simultaneous measurement of metabolites. The final product, pyruvate, was produced from glucose with an overall efficiency of 30%, which translates to an average conversion efficiency of 90% for each of the ten enzymatic steps involved. It was also found that a 10-fold increase in the amount of PfkA added to the complete reaction mixture led to a significant accumulation of intermediates F16P and dihydroxyacetone phosphate with a corresponding reduction in

G6P and F6P levels in the first half of the pathway. These observations support the hypothesis that additional copies of the rate-limiting PfkA enzyme can indeed enhance the F16P production rate of the constructed multi-enzyme complex.

In industry, economically viable biocatalytic conversions are limited to simple reactions performed by one or a few enzymes. This drawback is mainly linked to the high production costs of enzymes (Bell et al. 2021). Synthetic protein scaffolds are a promising avenue of investigation. In these systems, a cascade of enzymes is colocalised on a protein scaffold through well-characterised protein-protein interactions, resulting in a synthetic multi-enzyme complex. For example, Dueber et al. demonstrated a 77-fold increase in mevalonate yield in comparison with free-floating enzymes, utilising cells containing protein scaffolds (Dueber et al. 2009). Moreover, inclusion of a purification or immobilisation tag in the scaffold allows one-step purification, immobilisation and recycling of these self-assembling multi-enzyme complexes, as such drastically reducing production costs (Vanderstraeten and Briers 2020). Another benefit is the introduction of substrate channelling through the proximity effect between sequential enzymes. During substrate channelling, an intermediate produced in a pathway is more likely to be directly utilised as the substrate for the next enzyme (Zhang 2011). The main drawback of synthetic protein scaffolds is the labor-intensive process of protein tagging and genetic engineering. Consequently, the production of these multi-enzyme complexes is relatively time-consuming (Vazquez-Gonzalez et al. 2020). In addition, the concept of substrate channelling remains a subject of debate in vitro environments, highlighting the significant need for deeper insights on this matter (Abernathy et al. 2019). More extensive research is essential to fully understand why certain systems benefit from in vitro enzyme colocalisation, while others do not.

Since the glycolytic enzymes are well characterised, have been shown to colocalize under natural conditions and represent a primary pathway starting from cheap glucose, we have selected this pathway to serve as a model system to study the effects of in vitro pathway colocalization with a focus on the first three glycolytic enzymes from *E. coli* (Abernathy et al. 2017; Abernathy et al. 2019). By reinstalling the natural colocalization of co-operating enzymes, pathway efficiency may be increased in vitro (Vanderstraeten and Briers 2020). We utilise the highly efficient dockerin-cohesin interaction system from cellulosomes as protein-protein interaction pairs. Cellulosomes are naturally occurring multi-enzyme complexes created by specific microorganisms that consume plant cell wall carbohydrates. These complexes consist of a common backbone called a scaffoldin, which includes multiple tandem cohesin modules. (Hemi)cellulosic enzymes, responsible for degrading the plant cell wall, bind non-covalently to cohesins through dockerin modules. When an enzymatically active module is fused to a dockerin, it is generally referred to as a docking enzyme (Lamote et al. 2023). Since the discovery of cellulosomes in *Clostridium thermocellum*, they have served as a tool for engineering and constructing custom multi-enzyme complexes known as designer cellulosomes (Lamed et al. 1983; Vazana et al. 2012). In such a system, a chimeric scaffoldin containing cohesins from different organisms is combined with the ortholog dockerin modules fused to enzymatic modules. Since the cohesin-dockerin interaction is conserved within one species, they can serve as a

spatial colocalization tool with high binding affinity ($K_d=10^{-9}$ to 10^{-12} M) (Vanderstraeten and Briers 2020). Inspired by these systems, we constructed designer glycolysomes by colocalizing the first three glycolytic enzymes. We constructed different glycolytic docking enzymes and explored multiple chimeric scaffold designs to enhance F16P production. To construct the synthetic proteins, we harnessed the highly efficient VersaTile DNA assembly technique for rapid combinatorial construction of synthetic cohesin scaffolds and docking enzymes (Gerstmans et al. 2020; Vanderstraeten et al. 2022a; Vanderstraeten et al. 2022b).

2 | Experimental Procedures

2.1 | Bacterial Strains and Growth Media

E. coli TOP10 and *E. coli* BL21(DE3) RIL cells (Agilent Technologies, Belgium) were used for plasmid storage and protein expression, respectively. These strains were grown at 37°C in LB broth (1% (w/v) tryptone, 0.5% (w/v) yeast extract, 1% (w/v) NaCl) with shaking (180rpm) or on LB agar (1.5% (w/v) agar). For selection, LB was supplemented with 100 µg/mL ampicillin, 50 µg/mL kanamycin, 25 µg/mL chloramphenicol and/or 5% (w/v) sucrose (SacB counter-selection system). *E. coli* genomic DNA was extracted using the phenol/chloroform method as described by He (2011).

2.2 | VersaTile Cloning and Assembly

The DNA encoding enzymatically active modules was converted to Tiles as described by Vanderstraeten et al. (2022a). Tiles, DNA coding sequences for specific modules compatible with the VersaTile technique (Gerstmans et al. 2020), were constructed using primers from Integrated DNA Technologies (Table S1). VersaTile assembly was performed as described by Vanderstraeten et al. (2022a). Cohesin Tiles prepared to be fitted at the first, second, third and fourth positions include the cohesin-encoding domain followed by a sequence encoding a C-terminal linker. Cohesin Tiles prepared to be fitted at the fifth position do not include this linker sequence. In the case of Coh-*Cti* and Coh-*Ac*, part of the natural linker was included. The linker sequences have lengths of 41 and 6 amino acids, respectively. For Coh-*Af*, we included a synthetic linker of 5 amino acids (VVPST). This sequence was found in natural cellulosomal scaffolds (Vazana et al. 2013).

Similar to the cohesin Tiles, the *Ct*-CBM3 Tile includes a part of the C-terminal natural linker (36 amino acids) to fit at the first position. Table S2 visualises the 3-way assembly of synthetic docking enzymes, while Table S3 illustrates the 5-way assembly of chimeric scaffolds. In Figure S1, an overview of the used destination vectors is given.

2.3 | Small Scale Parallel Protein Expression and Western Blot

Overnight cultures were prepared by inoculating single colonies in separate wells of a 96-deep-well plate, with 500 µL LB, 50 µg/mL kanamycin and 25 µg/mL chloramphenicol. The plate was covered with air-permeable tape (Brand GmbH, Germany) and shaken (900rpm) at 37°C for 18h. Afterwards, 15 µL from

each well was transferred to a 96-deep-well plate filled with 500 µL of auto-induction medium (inducer: 0.2% (w/v) α -lactose) (Studier 2005), supplemented with 2 mM CaCl_2 per well. The plates were incubated at 37°C for 5 h (900 rpm), then at 16°C for 40 h (900 rpm). Cells were harvested by centrifugation (3200g, 30 min, 4°C), lysed with the BugBuster protein extraction reagent (Novagen), cleared by centrifugation (3200g, 45 min, 4°C), and stored at 4°C. Cleared lysates were analysed by 12% sodium dodecyl sulfate-polyacrylamide gel electrophoresis (SDS-PAGE) and Western blot using mouse Anti-His (Qiagen), rat Anti-Mouse IgG-Alkaline Phosphatase (Imtec) and nitro-blue tetrazolium chloride/5-bromo-4-chloro-3'-indolylphosphate p-toluidine salt (NBT/BCIP) (Sigma-Aldrich) as the detection reagent. Band intensity was analysed with the Bio-Rad Image Lab software.

2.4 | Large Scale Protein Expression and Purification

To express and purify the recombinant proteins, *E. coli* BL21(DE3) RIL cells, containing the correct vector, were grown at 37°C in LB, supplemented with 2 mM CaCl_2 . When OD_{600} reached 0.6, isopropyl thio- β -galactoside (IPTG) was added to a final concentration of 0.5 mM. After 18 h of incubation at 16°C and 180 rpm, cells were harvested by centrifugation (5 min, 20,000g) and resuspended in lysis buffer (Tris-buffered saline (TBS) (25 mM Tris-HCl; 137 mM NaCl; 3 mM KCl, pH 7.4), supplemented with 2 mM CaCl_2 and 40 mM imidazole). Cells were lysed by 1 mg/mL lysozyme, three freeze-thaw cycles and sonication (3 times 30s, 40% amplitude with 30s breaks) (Q125, Qsonica) on ice. The lysates were centrifuged (16,000g; 20 min) and filtered (Polyvinylidene difluoride (PVDF) membrane; 0.45 µm pore size).

His-tagged soluble proteins were purified by Immobilised Metal Affinity Chromatography (IMAC) with His GraviTrap columns (GE Healthcare, Belgium) according to the manufacturer's instructions. Samples were analysed by 12% SDS-PAGE, and protein concentrations were determined with the DeNovix DS-11 spectrophotometer. Extinction coefficients were calculated using ProtParam (Expasy).

2.5 | Native PAGE

A chimeric scaffold (100 pmol) was combined with synthetic docking enzyme (x pmol) in different molar ratios (0.6, 0.8, 1, 1.2, 1.4, 1.6) in a 30 µL reaction buffer (TBS, 10 mM CaCl_2 , 0.05% (v/v) Tween 20). The mixture was incubated at 37°C for 2 h or 18 h at 4°C. Half of the mixture was analysed on 10% native PAGE for 3 to 4 h at 100 volts, maintaining the container on ice to prevent sample denaturation.

2.6 | Enzymatic Activity Assays

For activity assays, enzyme complexes were prepared by mixing scaffold and docking enzyme(s) in equimolar amounts in TBS with 2 mM CaCl_2 , followed by incubation at 4°C for 16 h. Pairwise activity comparisons were conducted using proteins purified on the same day.

2.6.1 | Glucokinase (GlcK)

The substrate mixture consisted of 50 mM 3-(*N*-morpholino)propanesulfonic acid (MOPS) pH 7.4, 12 mM glucose, 4 mM ATP, 20 mM MgSO₄ and 2 mM CaCO₃. After preincubation at 37°C for 15 min, 2 pmol of enzyme was added to 1 mL of substrate mixture and further incubated at 37°C and 500 rpm. Samples of 100 μL were taken every 10 min for 1 h. Samples were immediately placed at 100°C for 5 min to inactivate the enzyme, after which the samples were stored on ice.

Conversion of substrate to product was evaluated by high-performance anion exchange chromatography—pulsed amperometric detection (HPAEC-PAD) with the Dionex ICS-3000 system (Thermo Fischer Scientific) (CarboPac PA20 column-3 × 150 mm) at a 0.5 mL flow rate. The protocol started with an isocratic elution with 30 mM of NaOH for 10 min. This was followed by a linear gradient for 2 min from 30 mM to 100 mM of NaOH. Additionally, NaOAc was similarly dosed to a final concentration of 200 mM. These conditions were kept constant for 15 min, after which initial conditions were restored in 2 min and maintained for 5 min. Glucose was detected after 5 min and glucose-6-phosphate (G6P) after 19 min. The glucose to G6P conversion was quantified using a 10–250 μM G6P standard curve. The concentration was calculated based on peak areas. Obtained slopes were converted to enzymatic activity (U/nmol).

2.6.2 | Phosphoglucose Isomerase (Pgi)

To accommodate the analysis in a larger number of samples, spectrophotometric assays were used to obtain the specific activity of *Ec*-Pgi and *Ec*-PfkA and their selected docking enzyme variants in bound and unbound states.

The substrate mixture consisted of 50 mM MOPS pH 7.4, 1.5 mM fructose-6-phosphate (F6P), 4 mM ATP, 20 mM MgSO₄ and 2 mM CaCl₂. After preincubation at 37°C for 15 min, 0.2 pmol enzyme was added to 2 mL substrate mixture and further incubated at 37°C and 500 rpm. Samples of 100 μL were taken every 5 min for 1 h. Samples were immediately placed at 100°C for 5 min to inactivate the enzyme, after which they were stored on ice.

The G6P detection was based on a method described by Jeong et al. (2003). Samples were supplemented with 800 μM NADP(+) and 0.25 U G6P dehydrogenase (Megazyme) in 96-well microtiter plates. The mixture was incubated at 25°C, and the absorbance at 340 nm (Tecan Plate Reader Infinite M Nano) was measured each minute until the plateau was reached. The amount of formed G6P was determined against a 0–250 μM G6P standard curve.

2.6.3 | Phosphofructokinase (PfkA)

The substrate mixture consisted of 50 mM MOPS pH 7.4, 2.5 mM F6P, 2.5 mM ATP, 20 mM MgSO₄ and 2 mM CaCl₂. After preincubation at 28°C for 15 min, 21 pmol of enzyme was added to 1.5 mL of substrate mixture and further incubated at 28°C and 500 rpm. Samples of 100 μL were taken every 4 min for 40 min.

The reaction was stopped by submersion of the samples in liquid nitrogen. Samples were then shortly stored at –20°C.

Since the enzymes were not heat-inactivated, the detection reaction was started immediately after thawing of the samples. For the calculation of formed F16P, samples were supplemented with 11 mM phosphoenolpyruvate (PEP), 312 μM NADH and 1 μL of pyruvate kinase (0.8 U/μL)—lactate dehydrogenase (1.2 U/μL) mixture for the determination of ADP from Sigma Aldrich (P0294) in 96-well microtiter plates. The mixture was incubated at 37°C, and the absorbance at 340 nm (Tecan Plate Reader Infinite M Nano) was measured each minute until the plateau was reached. The amount of formed F16P was determined using a 0–250 μM ADP standard curve.

2.6.4 | Glucokinase–Phosphoglucose Isomerase–Phosphofructokinase Pathway

The substrate mixture consisted of 50 mM MOPS pH 7.4, 1 mM glucose, 2.5 mM ATP, 20 mM MgSO₄ and 2 mM CaCl₂. After preincubation at 28°C for 10 min, 100 pmol of each enzyme (and scaffold) were added to 2 mL substrate mixture and further incubated at 28°C and 500 rpm. When multiple cohesin copies are introduced in the scaffold to accommodate several copies of *Ec*-PfkA docking enzyme, the enzyme concentration of *Ec*-PfkA is correspondingly increased to 200 and 300 pmol, respectively. Samples of 100 μL were taken every 10 min for 2 h. When 10 pmol (or 20–30 pmol for PfkA) of each enzyme (and scaffold) were added to the substrate mixture, samples were taken after 1, 2, 4, 6, 8 and 24 h. Samples were immediately placed at 100°C for 5 min to inactivate the enzymes, after which they were stored on ice.

The F16P detection method was based on a method described by Mesojednik and Legiša (2005). In short, samples were supplemented with 0.08 U aldolase (Sigma–Aldrich), 0.87 U triosephosphate isomerase (Sigma–Aldrich), 0.04 U glycerol-3-phosphate dehydrogenase (Sigma–Aldrich) and 1.1 mM NADH in 96-well microtiter plates. The mixture was incubated at 30°C, and the absorbance at 340 nm (Tecan Plate Reader Infinite M Nano) was measured each minute until the plateau was reached (Figure 1). The amount of formed F16P was determined against a 0–500 μM F16P standard curve.

2.7 | Data Processing

Spectrophotometric data were converted to product concentrations using a standard curve and adjusted with a negative control. Out-of-range data points were excluded. For specific enzymatic activity (U/mol), the slope of each replicate represented 1 μmol of product generated per minute (equivalent to 1 enzyme unit), divided by the protein concentration (mol) used. In the case of the designer glycolysomes, F16P product concentrations at each time point were determined. Mean and standard deviations were calculated from three replicates. Statistical analysis included ANOVA ($p < 0.05$) with Tukey HSD post hoc test ($p < 0.05$) for normally distributed (Shapiro–Wilk, $p > 0.05$) and homoscedastic (Levene's tests, $p > 0.05$) data, or Welch-ANOVA ($p < 0.05$) with Games–Howell post

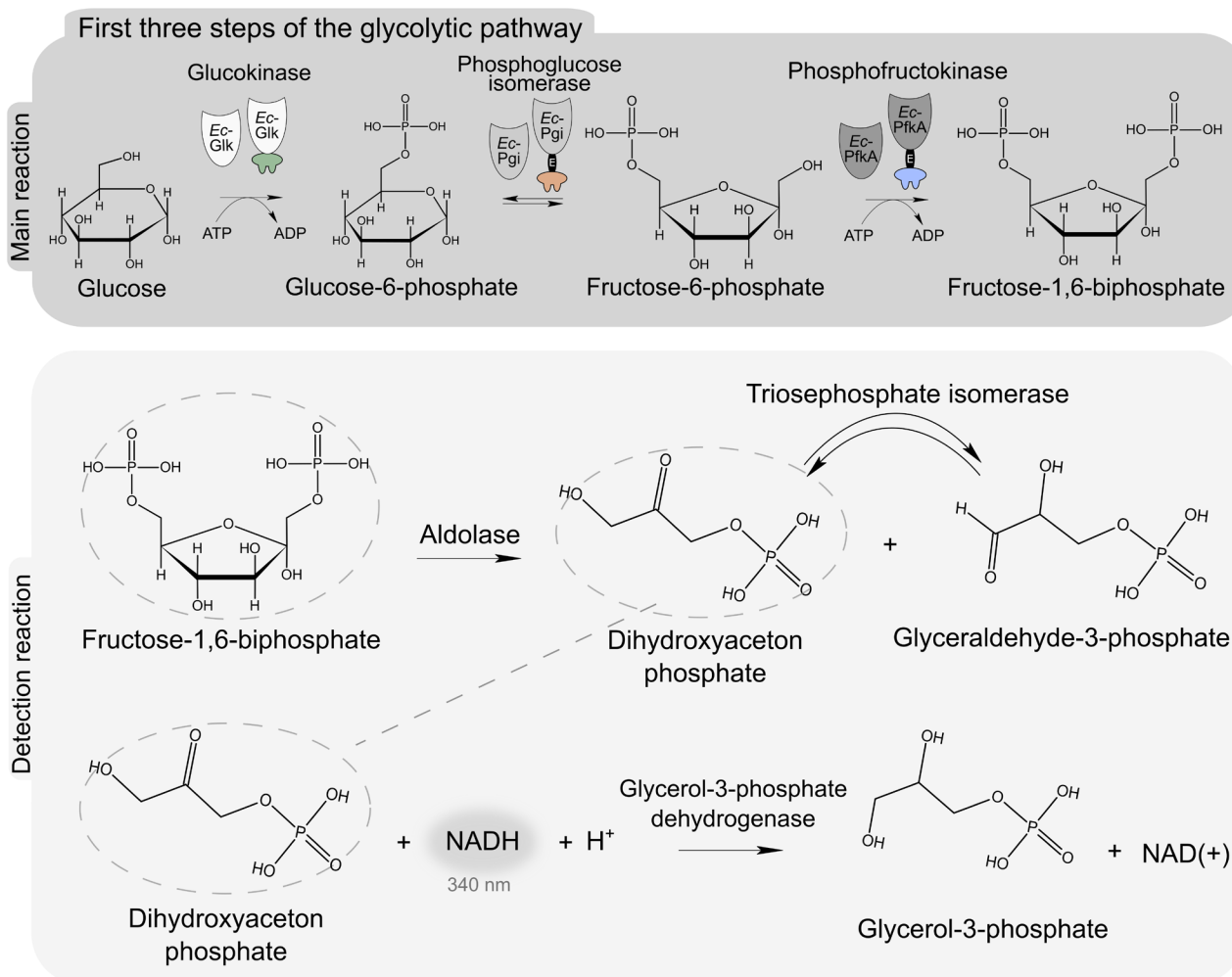


FIGURE 1 | Schematic overview of the activity assay used to determine the release of F16P by the combination of the first three glycolytic enzymes. In the main reaction, glucose is converted to F16P by the consecutive action of Glk, Pgi and PfkA. The released amount of F16P is then quantified in the detection reaction. First, F16P is converted to dihydroxyacetone phosphate and glyceraldehyde-3-phosphate by aldolase. Dihydroxyacetone phosphate is then reduced to glycerol-3-phosphate by glycerol-3-phosphate dehydrogenase. This results in the constant removal of dihydroxyacetone phosphate, thus ensuring the action of a third enzyme, triosephosphate isomerase, which converts glyceraldehyde-3-phosphate to dihydroxyacetone. Since glycerol-3-phosphate dehydrogenase performs an oxidation of NADH (spectrophotometric detection at 340 nm) to NAD, the reaction is quantifiable.

hoc test ($p < 0.05$) for non-normally distributed data. All data visualisation and statistical processing were conducted using R (version 4.4.1).

3 | Results

3.1 | Converting Wild-Type Glycolytic Enzymes to the Docking Enzyme Mode

As a proof of concept, the first three glycolytic enzymes—Glk, Pgi and PfkA—were selected to be incorporated in the synthetic protein scaffold. The first enzyme in the glycolytic pathway, Glk (Enzyme Commission [EC] number 2.7.1.2), is responsible for the phosphorylation of glucose to G6P by consuming ATP. The second step involves the isomerisation of G6P to F6P, catalysed by Pgi (EC 5.3.1.9). The third enzyme is Pfk (EC 2.7.1.11). This enzyme catalyses the conversion of F6P to F16P by consuming ATP. *E. coli* contains two Pfk isozymes, PfkA and PfkB. Since more than 90% of the Pfk activity in wild-type *E. coli* is

attributed to PfkA (Kotlarz and Buc 1982), this isozyme was selected to be converted to the docking enzyme mode. Together, these enzymes convert glucose into F16P (Figure 1).

To ensure proper colocalization of the glycolytic docking enzymes, organism-specific dockerin-cohesin pairs were selected from *C. thermocellum* (type 1 modules, CtI), *Archaeoglobus fulgidus* (Af) and *Acetivibrio cellulolyticus* (Ac). These pairs were chosen based on their lack of cross-reactivity, as confirmed in previous studies (Vanderstraeten et al. 2022a). Each glycolytic enzyme was assigned a unique dockerin to ensure precise spatial colocalization within the scaffold. Since we used a well-established cohesin set-up from Vanderstraeten et al. (2022a), Doc-CtI, Doc-Af and Doc-Ac were assigned to Ec-Glk, Ec-Pgi and Ec-PfkA, respectively. In constructing the synthetic docking enzymes, only C-terminal fusions were made between the enzymatic active module, a linker and a dockerin (Table S2), as the selected dockerins naturally occur at the C-terminus (Bayer et al. 2008; Bayer et al. 1999; Ding et al. 1999). This approach limited the combinatorial design space for each docking

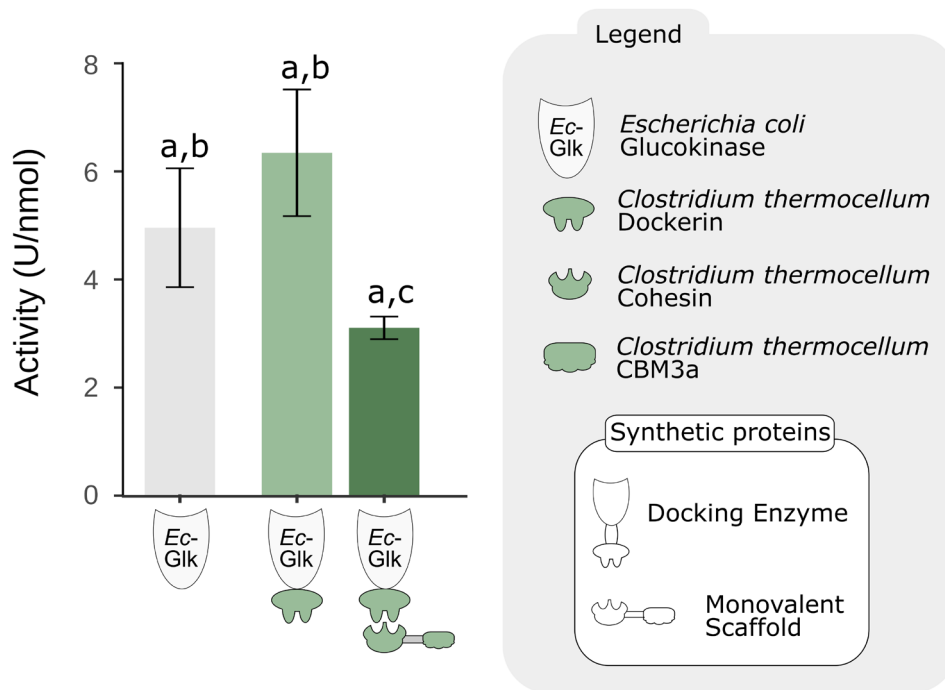


FIGURE 2 | Specific activity of *Ec*-Glc and its selected docking enzyme variant in bound and unbound states. The activity of *Ec*-Glc (construct nr. 1), *Ec*-Glc_*Doc*-*CtI* (construct nr. 2) and *Ec*-Glc_*Doc*-*CtI* (construct nr. 2) bound to *Ct*-CBM3_*Coh*-*CtI* (construct nr. 23) is shown. Dockerin fusion had no significant impact on the activity of the enzyme. Interaction with the cognate cohesin as part of a monovalent scaffold resulted in a 51% activity drop ($p < 0.05$). The letters above the bars indicate statistically significant differences between groups, as determined by one-way (Welch-) ANOVA followed by a post hoc test ($p < 0.05$). Bars sharing the same letter are not significantly different from each other, while bars with different letters represent groups with significant differences in enzymatic activity (U/nmol).

enzyme. The VersaTile DNA assembly technique facilitated rapid docking enzyme construction after making the glycolytic modules compatible with the available designer cellulosome Tile repository (Table S1). Expression levels, purification yields and enzymatic activities were evaluated for each dockerin fusion. Furthermore, monovalent scaffolds were created to test the binding efficiency of the docking enzymes and the effect of this binding on their enzymatic activity.

The monovalent scaffolds were composed of *C. thermocellum* CipA carbohydrate-binding module 3 (*Ct*-CBM3) and a cohesin module (*Coh*-*CtI*, *Coh*-*Af* or *Coh*-*Ac*) for constructs 23, 24 and 25, respectively (Table S3), and displayed high expression levels. SDS-PAGE analysis of these IMAC-purified samples revealed distinct bands for the target proteins (Figure S2). While *Ct*-CBM3_*Coh*-*CtI* is monomeric, *Ct*-CBM3_*Coh*-*Af* and *Ct*-CBM3_*Coh*-*Ac* show both monomeric and dimeric bands. Wild-type *Ec*-Glc, *Ec*-Pgi and *Ec*-PfkA enzymes were fused to a C-terminal His-tag (construct nr. 1, 3 and 13, respectively, Table S2) and showed high purification levels after SDS-PAGE analysis of IMAC-purified samples (Figure S3). The *Ec*-Glc docking enzyme (*Ec*-Glc_*Doc*-*CtI*, construct nr. 2, Table S2) yielded highly expressible protein (Figure S4). Native PAGE analysis confirmed spontaneous complex formation with its monovalent scaffold (*Ct*-CBM3_*Coh*-*CtI*) (Figure S5). The Glc activity assay (Figure 2) showed no significant difference ($p > 0.05$) between natural *Ec*-Glc (4.96 ± 1.10 U/nmol) and unbound *Ec*-Glc_*Doc*-*CtI* (6.34 ± 1.17 U/nmol). However, binding the *Ec*-Glc docking enzyme to the monovalent scaffold (CBM3_*Coh*-*CtI*) reduced its activity by 51% (3.11 ± 0.21 U/nmol, $p < 0.05$).

For *Ec*-Pgi and *Ec*-PfkA, direct dockerin fusions (construct nr. 4 and 14, respectively, Table S2) did not yield recombinant protein (data not shown), prompting optimisation through the addition of linkers between the enzymatically active domain and the dockerin. Eight different linkers, A until H, were selected, with varying flexibility and polarity and can be found in the Supporting Information (Table S4). The new docking variants were expressed on a small scale, and the resulting lysates were analysed by SDS-PAGE and Western blot analysis (Figures S6 and S7). For *Ec*-Pgi, the two highest-expressing constructs (*Ec*-Pgi_*Li*-*E*-*Doc*-*Af*, construct nr. 9 and *Ec*-Pgi_*Li*-*H*-*Doc*-*Af*, construct nr. 12) encompass a flexible linker (Linker E: [GGGG]₃) and a rigid linker (Linker F: [AP]₃). In contrast, the two highest-expressing *Ec*-PfkA docking constructs (*Ec*-PfkA_*Li*-*E*-*Doc*-*Ac*, construct nr. 19, and *Ec*-PfkA_*Li*-*F*-*Doc*-*Ac*, construct nr. 20) both harbour flexible linkers (Linker E: [GGGG]₃, Linker F: [G]₈). Large-scale expression of these four proteins confirmed high IMAC-purification levels after SDS-PAGE analysis (Figures S8 and S9). Native PAGE demonstrated effective interaction with the corresponding monovalent cohesin scaffolds (Figures S10 and S11).

The enzymatic activity of the natural *Ec*-Pgi enzyme (49.43 ± 0.81 U/nmol) (Figure 3) was significantly higher ($p < 0.05$) than that of the unbound docking enzymes (*Ec*-Pgi_*Li*-*E*-*Doc*-*Af*: 15.50 ± 0.66 U/nmol and *Ec*-Pgi_*Li*-*H*-*Doc*-*Af*: 15.83 ± 0.64 U/nmol). Fusing the enzyme to a dockerin via a linker caused a substantial drop in activity of 69% ($p < 0.05$) and 68% ($p < 0.05$), respectively. When bound to the monovalent scaffold, activity decreased by an additional 29% ($p < 0.05$).

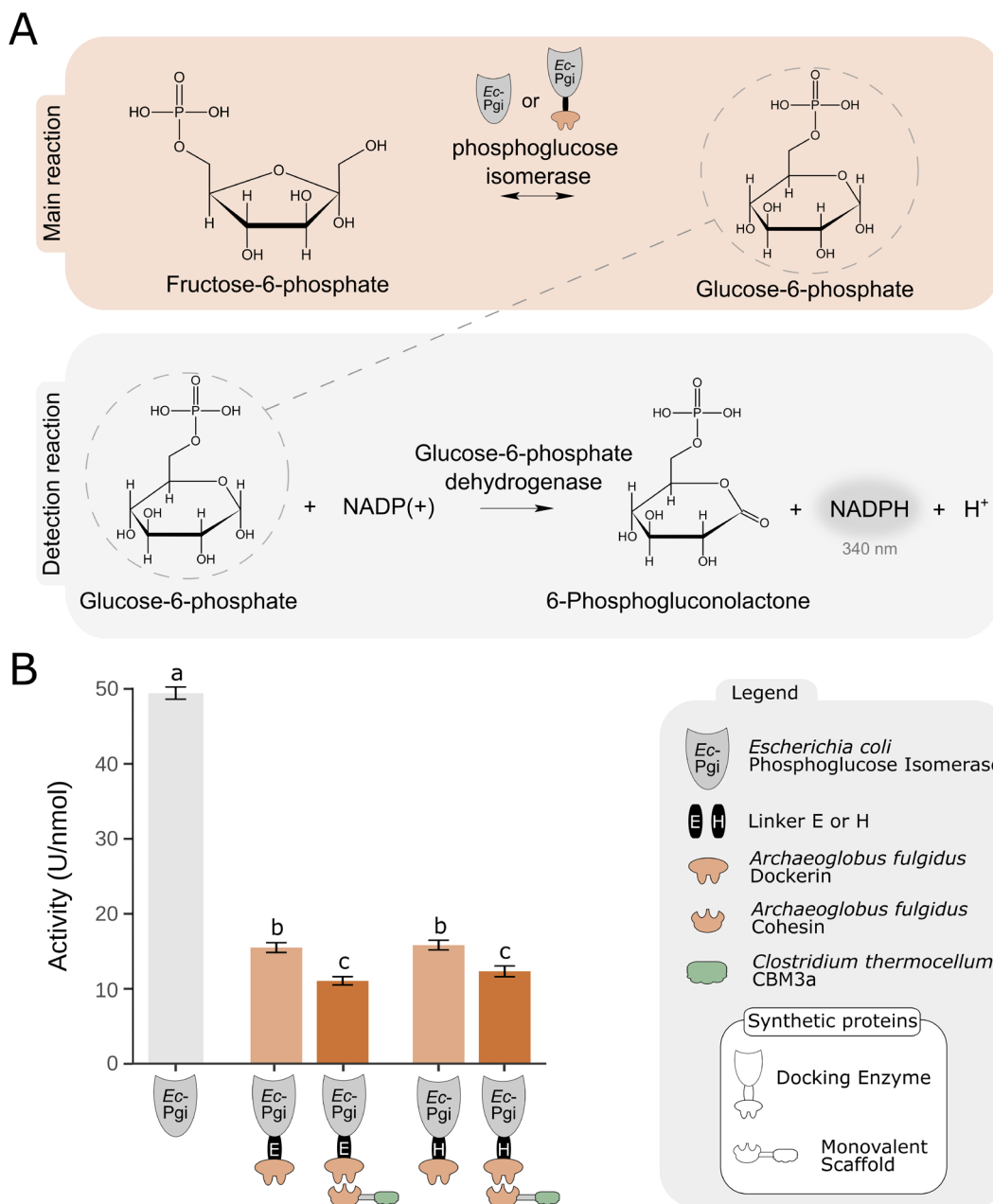


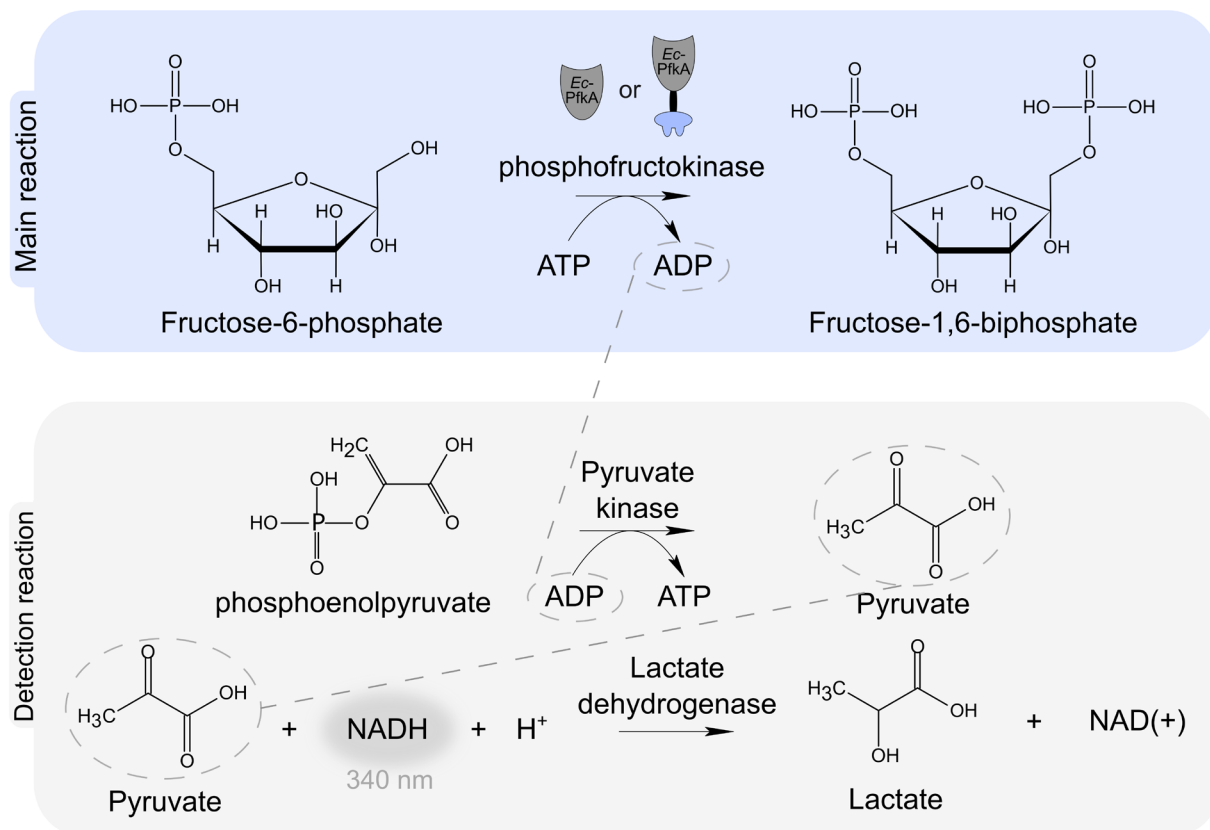
FIGURE 3 | (A) Schematic overview of Pgi activity assay. In the main reaction, Pgi isomerizes F6P to G6P. The amount of G6P formed in the main reaction is then quantified in the detection reaction. Here, G6P dehydrogenase oxidises G6P and reduces NADP(+) to 6-phosphogluconolactone and NADPH, respectively. The amount of released NADPH can be measured spectrophotometrically (340 nm) and is directly correlated to the amount of G6P formed in the main reaction. (B) Specific activity of *Ec*-Pgi and its selected docking enzyme variants in bound and unbound states. The activity of *Ec*-Pgi (construct nr. 3), *Ec*-Pgi_Li-E_Doc-Af (construct nr. 9), *Ec*-Pgi_Li-E_Doc-Af (construct nr. 9) bound to *Ct*-CBM3_Coh-Af (construct nr. 24), *Ec*-Pgi_Li-H_Doc-Af (construct nr. 12) and *Ec*-Pgi_Li-H_Doc-Af (construct nr. 12) bound to *Ct*-CBM3_Coh-Af (construct nr. 24) are shown. Dockerin fusion caused a considerable drop in activity (68%–69%). Interaction of the *Ec*-Pgi docking enzymes with the monovalent scaffold resulted in an additional drop in activity of approximately 29% and 22%. There is no significant difference in specific activity between the two selected docking enzymes, either in unbound or bound states. The letters above the bars indicate statistically significant differences between groups, as determined by one-way (Welch-)ANOVA followed by a post hoc test ($p < 0.05$). Bars sharing the same letter are not significantly different from each other, while bars with different letters represent groups with significant differences in enzymatic activity (U/nmol).

and 22% ($p < 0.05$) for *Ec*-Pgi_Li-E_Doc-Af (11.07 ± 0.55 U/nmol) and *Ec*-Pgi_Li-H_Doc-Af (12.33 ± 0.72 U/nmol), respectively. There was no significant difference ($p > 0.05$) in specific activity between the two bound docking enzymes. Taking into account possible steric clashes in the full designer

glycolysome, we selected the docking enzyme with a flexible linker (*Ec*-Pgi_Li-E_Doc-Af).

The natural *Ec*-PfkA exhibited a specific activity of 0.153 ± 0.014 U/nmol (Figure 4), which was notably lower

A



B

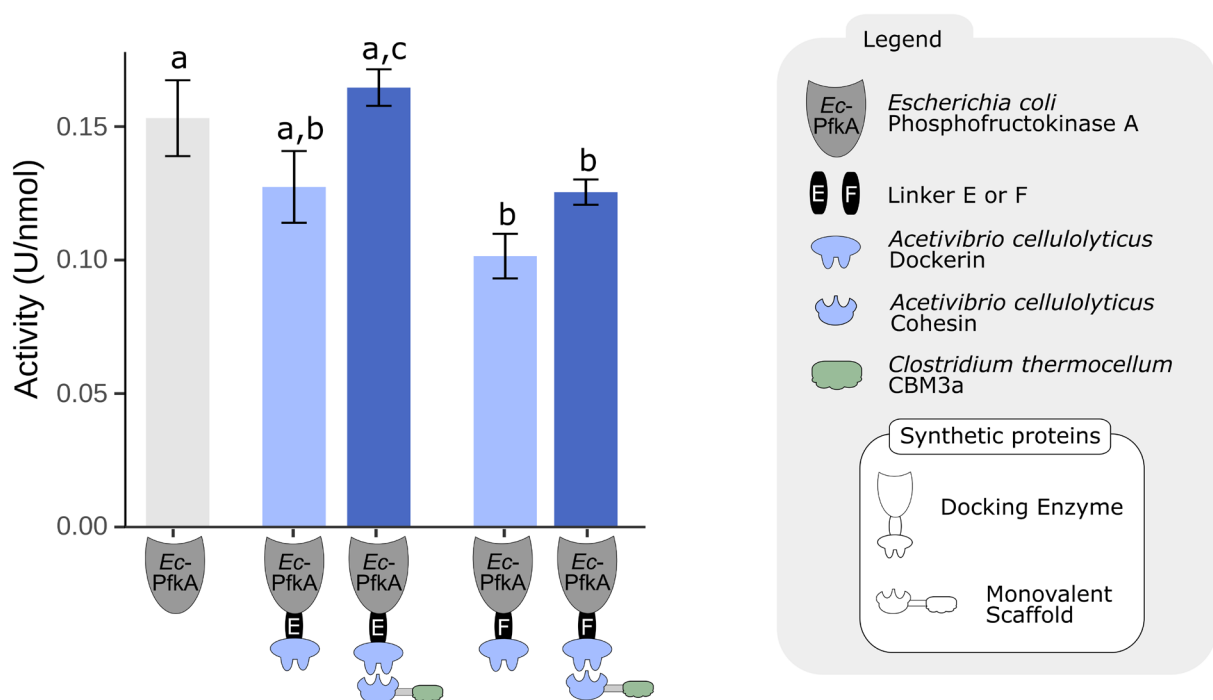


FIGURE 4 | Legend on next page.

than the activities of the previous enzymes. Attaching the *Ec-PfkA* catalytic module to a dockerin through a linker led to a reduction in specific activity. *Ec-PfkA*_Li-E_Doc-Ac showed a non-significant decrease of 17% (0.127 ± 0.013 U/nmol, $p > 0.05$), while *Ec-PfkA*_Li-F_Doc-Ac displayed a significant 34% drop (0.101 ± 0.008 U/nmol, $p < 0.05$). There was no

significant difference ($p > 0.05$) in the specific activity between both unbound docking enzymes. Interestingly, when the docking enzymes interacted with the monovalent scaffold, their performance improved again. *Ec-PfkA*_Li-E_Doc-Ac exhibited a 30% increase in activity (0.165 ± 0.007 U/nmol, $p < 0.05$), while *Ec-PfkA*_Li-F_Doc-Ac improved by 24% (0.125 ± 0.005 U/

FIGURE 4 | (A) Schematic overview of PfkA activity assay. During the main reaction, PfkA catalyses the conversion of F6P and ATP to F16P and ADP. In the following detection reaction, the released ADP is used to dephosphorylate PEP by pyruvate kinase. Subsequently, lactate dehydrogenase reduces pyruvate and oxidises NADH to lactate and NAD(+), respectively. The amount of NADH present in the reaction mixture can be measured spectrophotometrically (340nm) and is inversely correlated to the amount of F16P released in the main reaction. (B) Specific activity of *Ec*-PfkA and its selected docking enzyme variants in bound and unbound states. The activity of *Ec*-PfkA (construct nr. 13), *Ec*-PfkA_Li-E_Doc-Ac (construct nr. 19), *Ec*-PfkA_Li-E_Doc-Ac (construct nr. 19) bound to *Ct*-CBM3_Coh-Ac (construct nr. 25), *Ec*-PfkA_Li-F_Doc-Ac (construct nr. 20) and *Ec*-PfkA_Li-F_Doc-Ac (construct nr. 20) bound to *Ct*-CBM3_Coh-Ac (construct nr. 25) are shown. Dockerin fusion caused a 17% and 34% activity drop, respectively. There is no significant difference in specific activity between the two selected docking enzymes in the unbound state. Interaction of the docking enzymes with the cognate cohesin as part of a monovalent scaffold causes a significant increase in specific activity of 30% for *Ec*-PfkA_Li-E_Doc-Ac and a non-significant increase of 24% for *Ec*-PfkA_Li-F_Doc-Ac. The highest specific activity was detected for *Ec*-PfkA_Li-E_Doc-Ac (construct nr. 19) bound to *Ct*-CBM3_Coh-Ac (construct nr. 25). The letters above the bars indicate statistically significant differences between groups, as determined by one-way (Welch-)ANOVA followed by a post hoc test ($p < 0.05$). Bars sharing the same letter are not significantly different from each other, while bars with different letters represent groups with significant differences in enzymatic activity (U/nmol).

nmol, $p > 0.05$). The specific activities of the bound enzymes differed significantly ($p < 0.05$) from each other. We hypothesise that scaffold multimerisation, as illustrated in Figure S2 (lower panel), facilitates the formation of super complexes. Care must be taken when constructing the full designer glycolysome. Despite both linkers (Linker E: [GGGS]₃ and Linker F: [G]₈) being flexible, they differ in length, with Linker E being longer. This increased length may enhance the separation between the dockerin and the catalytic module, possibly resulting in a higher activity when bound in the full glycolytic complex. With this in mind and based on the activity assay, *Ec*-PfkA_Li-E_Doc-Ac was retained as the optimal *Ec*-PfkA docking enzyme variant.

3.2 | Construction and Activity Analysis of the Trivalent, Tetravalent and Pentavalent Glycolytic Enzyme Complexes

Based on the activity assays performed on the separate docking enzyme variants, three docking enzymes were selected to be incorporated in the multi-enzyme complex: *Ec*-Glk_Doc-CtI (construct nr. 2), *Ec*-Pgi_Li-E_Doc-Af (construct nr. 9) and *Ec*-PfkA_Li-E_Doc-Ac (construct nr. 19). Since each docking enzyme carries a dockerin originating from a different micro-organism, they can be spatially colocalized in a multi-enzyme complex by interaction with a trivalent scaffoldin, composed of the three cognate cohesin modules. We thus constructed a trivalent scaffold, composed of a *Ct*-CBM3, *Coh*-CtI, *Coh*-Af and *Coh*-Ac (construct nr. 26). Given that PfkA exhibits the lowest activity (Figure 4B), PfkA is expected to be the rate-limiting enzyme in this series of pathway enzymes. We explored the inclusion of extra copies of PfkA in the scaffolded multi-enzyme complex by incorporating more *Coh*-Ac modules. Consequently, two additional scaffolds were constructed: a tetravalent scaffold that has the capacity for an extra copy of PfkA (construct nr. 27), while the pentavalent scaffold can accommodate two additional copies of PfkA (construct nr. 28). SDS-PAGE analysis of the IMAC-purified elutions of the three scaffolds can be found in the Supporting Information (Figure S12).

A reaction mixture containing glucose and ATP was supplemented with 100 pmol *Ec*-Glk_Doc-CtI, *Ec*-Pgi_Li-E_Doc-Af and *Ec*-PfkA_Li-E_Doc-Ac. The docking enzymes were added either unbound or as part of the trivalent, tetravalent or pentavalent enzyme complex. In the case of the tetravalent or

pentavalent enzyme complex, 200 and 300 pmol *Ec*-PfkA_Li-E_Doc-Ac were added, respectively. ATP has been reported to have an inhibitory effect on PfkA (Zheng and Kemp 1992). A fixed concentration of 2.5 mM ATP (as was used to verify the activity of the *Ec*-PfkA docking enzymes) was therefore used to test the combination of the three docking enzymes. In the selected pathway, both *Ec*-Glk and *Ec*-PfkA consume ATP. However, *Ec*-Glk has a much greater turnover number, as shown in this research. By including a minimal amount of glucose (1 mM), we restrict the number of ATP molecules that can be used by *Ec*-Glk and ensure the presence of ATP molecules necessary for *Ec*-PfkA activity. We note that 1 mM glucose does not correspond to saturated substrate conditions for the *Ec*-Glk enzyme.

The activity analysis revealed that the constructed multi-enzyme complexes are able to perform the first three steps of glycolysis and convert glucose into F16P (Figure 5). There was no significant difference ($p < 0.05$) between the production rate of the pathway colocalized on the trivalent, tetravalent or pentavalent scaffold when compared to an equimolar mixture of docking enzymes, indicating that the selected enzymes do not benefit from being colocalized at high enzyme concentrations. Yet, this also indicates that the incorporation of the three enzymes in the complex does not cause a significant drop in pathway efficiency in spite of the observed reductions of the activity of the single enzymes upon dockerin fusion and/or docking, as observed for *Ec*-Glk and *Ec*-Pgi. Following the docking enzyme activity screening, *Ec*-PfkA is expected to be the rate-limiting enzyme in this sequence of pathway enzymes. Indeed, when an additional copy of *Ec*-PfkA is introduced, doubling the number of copies, the production rate also doubles. The tetravalent complex (4.78 ± 0.14 nmol/min) produced nearly twice as much F16P as the trivalent complex (2.86 ± 0.20 nmol/min), reinforcing that PfkA is the rate-limiting enzyme. Similarly, the pentavalent complex (7.41 ± 0.78 nmol/min) showed a 1.5-fold increase over the tetravalent complex and a threefold increase over the trivalent complex in F16P production. These results suggest that the pathway benefits from the inclusion of additional copies of PfkA. Likewise, a similar pattern is observed with the free docking enzymes, resulting in production rates of 2.88 ± 0.13 , 4.94 ± 0.19 and 7.30 ± 0.74 nmol/min for the 1× PfkA, 2× PfkA and 3× PfkA scenarios, respectively.

Colocalization effects may be most outspoken under limited substrate concentrations (Vanderstraeten et al. 2022b).

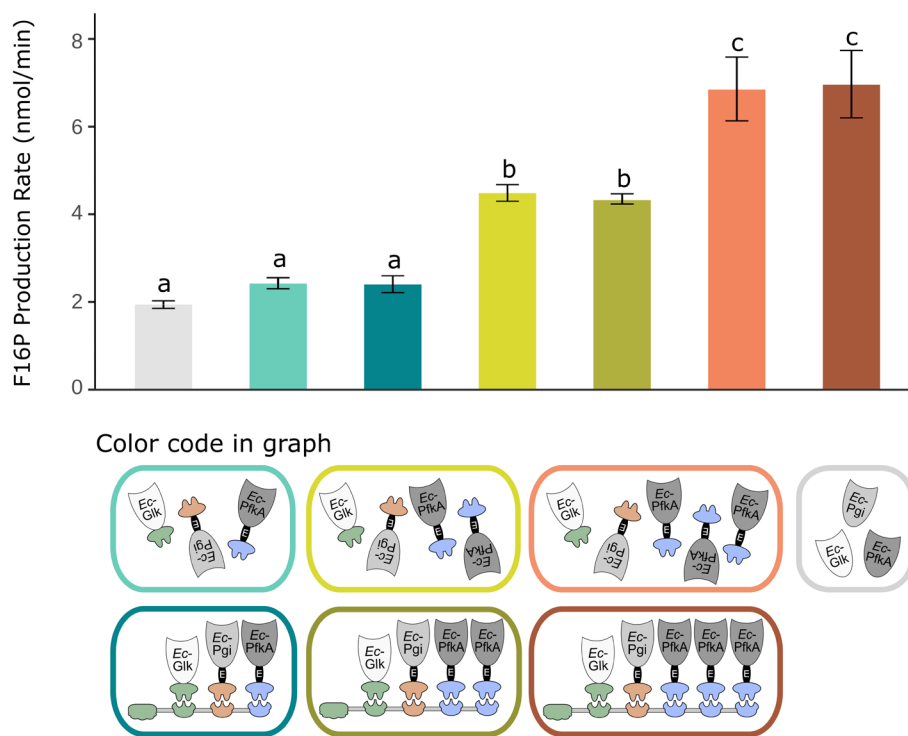


FIGURE 5 | Standard activity analysis of the synthetic protein complexes composed of the first three *E. coli* glycolytic enzymes. The production rate of the trivalent, tetravalent or pentavalent complexes is shown. They are able to perform the first three steps of glycolysis and convert glucose into F16P. There was no significant difference between the production rate of the pathway colocalised on the trivalent, tetravalent or pentavalent complex compared to an equimolar mixture of docking enzymes. Increasing the copy number of *Ec-PfkA_Li-E_Doc-Ac* increased the production of F16P in a copy number-dependent way. Each bar represents the mean \pm standard deviation of three replicates. Statistically significant differences between groups were assessed using one-way ANOVA followed by a post hoc test ($p < 0.05$). Bars sharing the same letter indicate no significant difference, whereas bars with different letters signify significant differences.

Therefore, an activity assay was conducted using a pentavalent complex and an equimolar mixture of docking enzymes at a substrate concentration lowered by a factor of 2 (0.5 mM glucose). However, no significant difference was observed in the amount of F16P produced between the pentavalent complex and the equimolar mixture of docking enzymes (Figure S13) (Yoon et al. 2012).

It has also been suggested that proximity effects are less significant in vitro at high enzyme densities (Chado et al. 2016; Yong et al. 2020). We thus repeated the assay with a ten times lower amount of each enzyme (10 pmol) and a longer incubation time (24 h) (Figure 6). Indeed, prominent colocalization effects were observed under these conditions, and the amount of F16P produced by both the trivalent (from 4 h) and pentavalent (from 1 h) complex was significantly higher ($p < 0.05$) than the amount produced by an equimolar mixture of docking enzymes. After one hour, the percentage increase in F16P production due to scaffolding is much greater in the pentavalent complex scenario (571%) than in the trivalent complex scenario (215%). As time progresses, the effect of colocalization on F16P production becomes more pronounced in the trivalent complex (1x *Ec-PfkA*), showing a 248% increase at two hours compared to an equimolar mix of free docking enzymes. In contrast, the pentavalent complex (3x *Ec-PfkA*) shows only a 57% increase at the same time point when compared to the same free docking enzyme mix.

4 | Discussion

The effect of in vitro colocalization on pathway enzymes is not yet fully understood. Although in some cases major activity enhancements have been detected, improvements were minor or non-existent in others. More research is needed to fully comprehend the effects of bringing pathway enzymes in close proximity. However, since the construction and optimisation of these multi-enzyme complexes is a multiparametric process (selection of enzymes, choice of docking system, architecture, composition, linker, etc.), these studies are relatively complex. Here, the VersaTile DNA assembly technique allowed us to efficiently construct multiple docking enzyme variants and scaffolds, as such exploring the colocalization effect between the first three glycolytic enzymes.

We successfully converted the first three enzymes of the natural *E. coli* glycolytic pathway into docking enzymes. Overall, converting natural enzymes to the docking enzyme mode can cause a substantial drop in activity. For the docking enzymes of *Ec-Pgi* and *Ec-PfkA*, successful protein expression was only achieved when the enzymatically active module was separated from the docking domain by a linker. We selected two variants containing flexible linkers (*Ec-Pgi_Li-E_Doc-Af* and *Ec-PfkA_Li-H_Doc-Ac*). As such, both modules may remain relatively mobile upon incorporation in the full multi-enzyme complex (Chen et al. 2013).

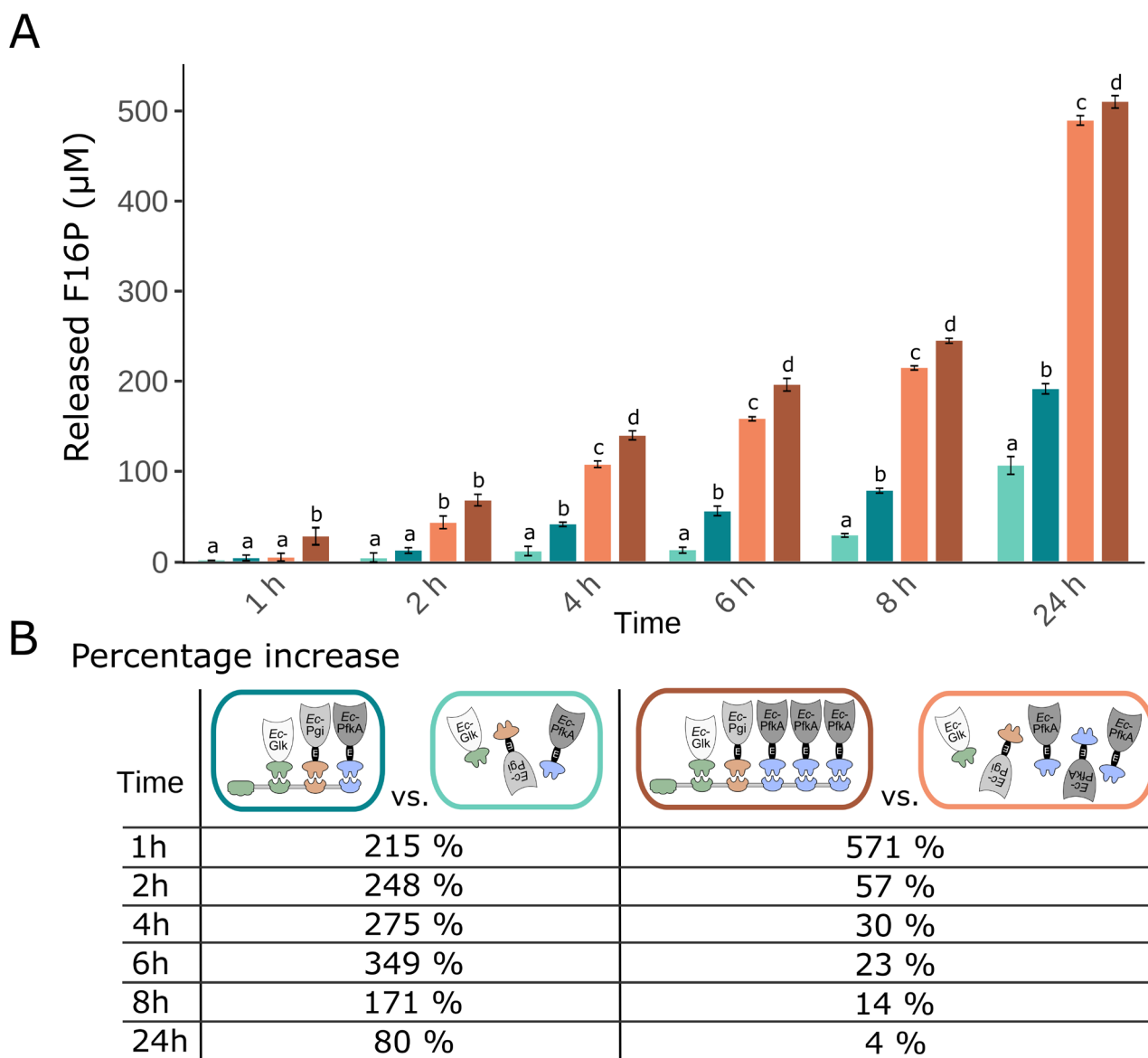


FIGURE 6 | (A) Activity assay with ten times lower enzyme densities and a longer incubation time (24h) than the standard activity assay. The amount of F16P produced by both the trivalent (from 4h) and pentavalent (from 1h) complex was significantly higher ($p < 0.05$) than the amount produced by an equimolar mixture of docking enzymes. Each bar represents the mean \pm standard deviation of three replicates. Statistically significant differences between groups were assessed using one-way ANOVA followed by a post hoc test ($p < 0.05$). Bars sharing the same letter indicate no significant difference, whereas bars with different letters signify significant differences. The statistical analysis is valid only within the different time points. (B) The percentage difference between the complexed and free enzymes, which serves as an indicator of the colocalization effect, shows that the complexes outperform the free enzymes. The percentage increase between the complexed and free enzymes—and thus the colocalization effect—diminishes in both the pentavalent and trivalent complexes (the decrease begins from 8 h for the trivalent complex and from 2 h for the pentavalent complex).

For *Ec*-Glk, the docking enzyme could be constructed by direct C-terminal fusion between the enzymatically active module and the dockerin. Moreover, the activity of the *Ec*-Glk docking enzyme did not significantly differ from the natural enzyme. However, binding of this docking enzyme to a monovalent scaffold led to the most drastic activity drop (-51%) observed among all tested docking enzymes. Presumably, the interaction between the dockerin and cohesin induces a conformational change in the entire protein or increases steric hindrance, leading to the observed activity drop. Possibly, the insertion of a linker sequence could provide distancing between the two protein domains, as

such limiting the activity drop and revealing the advantage of a linker sequence at this level (Kahn et al. 2019). The largest activity drop, caused by dockerin fusion, was detected for *Ec*-Pgi_Li-E_Doc-Af (-69%). However, the bound *Ec*-Pgi docking enzyme remains highly active, exhibiting a specific activity that is 3.6 times higher than that of bound *Ec*-Glk_Doc-Ctl and 67 times higher than bound *Ec*-PfkA_Li-E_Doc-Ac. Therefore, the *Ec*-PfkA docking enzyme is the rate-limiting enzyme in this pathway series. This is expected, as PfkA catalyses the first committed step in glycolysis and its activity is tightly regulated in nature (Guitart Font and Sprenger 2020).

When we compare the amount of F16P released by the tri-, tetra- and pentavalent complex to the amount released by the equimolar mixture of docking enzymes at high enzyme concentrations, we observe no significant difference between the production rates. This indicates that the interaction of each docking enzyme with the trivalent scaffold did not result in a drop in overall pathway efficiency. However, when we examined the activity of the separate docking enzymes in both bound and unbound conditions, the activity loss caused by the interaction of the docking enzyme with a monovalent scaffold was significant for both *Ec-Glk_Doc-Ctl* and *Ec-Pgi_Li-E_Doc-Af*. In the case of *Ec-PfkA_Li-E_Doc-Ac*, the activity actually increased upon interaction with a monovalent scaffold. We cannot draw conclusions about the effect of the interaction of the separate docking enzymes with the tri-, tetra- and pentavalent scaffold without monitoring the amount of each intermediate during the assay. It is plausible that the interaction with the tri-, tetra- and pentavalent scaffold causes similar effects to those observed for the monovalent scaffold, but that these effects may cancel each other. In any case, in vitro colocalization does not offer the enzymes a clear benefit in terms of production rate when high enzyme concentrations are used; however, the scaffold holds its potential for immobilisation and recycling of the complex (Roberts et al. 2021). The tetravalent complex produced twice as much F16P as the trivalent complex. Similarly, the pentavalent complex exhibited a 1.5-fold increase and a threefold increase in F16P production, compared to the tetravalent and trivalent complexes, respectively. This pattern is also observed with the free docking enzymes. These findings further support the role of PfkA as the rate-limiting enzyme and show that incorporating additional copies of PfkA enhances the production rate.

Since *Ec-PfkA_Li-E_Doc-Ac* is the rate-limiting enzyme, we anticipate that a single copy of the enzyme will not be able to convert the influx of F6P provided by the upstream *Ec-Pgi_Li-E_Doc-Af*. Operating at 100 pmol will result in the accumulation of F6P, the substrate for the PfkA enzyme, which will diffuse into the bulk of the reaction mixture. Consequently, *Ec-PfkA_Li-E_Doc-Ac*, when incorporated into the multi-enzyme complex, offers no advantage over the same docking enzyme acting freely in the mixture.

Lowering the enzyme quantity aims to avoid the absolute accumulation and diffusion of G6P to the bulk of the reaction. Indeed, when performing the assay with a tenfold lower enzyme amount (10 pmol), the scaffold provides the advantage of enzyme proximity and shows substrate channelling. This effect reduces the absolute likelihood of F6P diffusion into the bulk, making it more readily available for scaffolded *Ec-PfkA*. The colocalization effect was observed when comparing the trivalent and pentavalent complex with an equimolar mixture of docking enzymes. This demonstrates that at lower enzyme densities, the proximity effects provided by scaffolding result in a higher production yield compared to non-scaffolded docking enzymes. The enhancement in F16P production due to scaffolding depends on various factors. Specifically, time plays a crucial role.

In the beginning (after 1 h), the F16P production increase due to scaffolding is more pronounced in the pentavalent complex

scenario (3× *Ec-PfkA*) (571%) compared to the trivalent complex scenario (1× *Ec-PfkA*) (215%). However, at later time points, the opposite is observed, and the percentage increase in F16P production becomes greater in the trivalent complex scenario than in the pentavalent complex scenario. As time progresses, the percentage difference diminishes in both the pentavalent and trivalent complexes (the decrease begins from 8 h for the trivalent complex and from 2 h for the pentavalent complex). Interestingly, the percentage for the pentavalent complex decreases more rapidly than for the trivalent complex.

A possible explanation for these results may be due to the relative abundance of PfkA compared to its available substrate. In the beginning of the reaction, the preceding enzymes did not have sufficient time to produce F6P, so in both cases, the produced F6P will not diffuse into the bulk. Since there are three times as much PfkA present in the pentavalent complex, the more pronounced scaffolding lies solely in the increased presence of PfkA (3×10 pmol), elevating F16P production attributed to scaffolding. At later time points, the preceding enzymes could have already produced a sufficient amount of F6P, leading to its diffusion into the bulk of the reaction. In the scenario involving the pentavalent complex (3× *Ec-PfkA*) versus the free equimolar mixture of docking enzymes, the free mixture also includes 30 pmol of *Ec-PfkA*. This higher concentration of PfkA increases the likelihood of the enzyme encountering diffused F6P, resulting in a faster conversion to F16P, which reduces the difference between the scaffolded and free enzyme activities. Conversely, in the scenario involving the trivalent complex (1× *Ec-PfkA*) versus the free equimolar mixture of docking enzymes, only 10 pmol of PfkA is present in the free mixture. This lower concentration decreases the probability of PfkA encountering diffused F6P, leading to a slower conversion to F16P and, consequently, a greater difference between the scaffolded and free enzyme activities.

An alternative hypothesis for the diminishing increase in F16P production resulting from scaffolding in both the pentavalent and trivalent scenarios may be related to complex stability. Since the colocalization effect of the pentavalent complex decreases more rapidly than that of the trivalent complex, we speculate that this may be attributed to the larger size of the pentavalent complex, which could render it more prone to degradation. Future studies should focus on investigating the stability of these enzyme complexes under different conditions, as this represents a valuable opportunity for further optimisation.

However, the potential stability of enzyme colocalization within synthetic scaffolds over time is an important consideration. While our enzyme activity assays suggest that colocalization is maintained over a 24-h period, further experimental validation is needed to confirm stable interactions over extended timeframes. Determining the long-term viability of scaffolded enzyme systems is crucial for practical applications in biocatalysis and other synthetic biology fields.

An important question is whether enzyme colocalization offers tangible benefits for industrial applications. Based on our research, colocalization appears to be effective only at lower enzyme concentrations for this particular enzyme complex. If free enzymes exhibit limited stability while colocalized enzymes

demonstrate enhanced stability, adopting a strategy that employs longer incubation times with lower concentrations of colocalized, stable enzymes could be advantageous. This approach may outperform the use of shorter incubation times with higher concentrations of free, less stable enzymes.

Furthermore, utilising lower concentrations of colocalised enzymes could be particularly advantageous in scenarios where the cost of enzyme production and purification is a significant consideration. This strategy not only reduces the amount of enzyme required but also enables the recycling of enzyme complexes, offering additional cost-efficiency and sustainability benefits for industrial processes. All these cost-related aspects should be counterbalanced with the cost of reactor usage, which will increase when the reactor time increases.

There is an ongoing debate regarding the precise mechanism driving the enhancement from colocalization, with some researchers arguing that the proximity of enzymes may not necessarily prevent diffusion of intermediates into the bulk solution, as the diffusion rate of small molecules is typically faster than enzyme catalysis (Ledesma-Fernandez et al. 2023). Bauler et al. argued that proximity channelling, where intermediates are processed by a nearby enzyme before diffusing away, is unlikely to be effective because intermediates must approach within 0.1–1 nm of an enzyme's active site, making productive channelling improbable even when enzymes are approximately 10 nm apart (Bauler et al. 2010). To address the paradox of improved metabolic yields from scaffolds despite these limitations, Castellana et al. proposed a model where multiple copies of upstream and downstream enzymes form compact agglomerates. These clusters significantly increase the likelihood of intermediates being processed by downstream enzymes, mimicking the efficiency of direct channelling without the need for a physical tunnel (Castellana et al. 2014). Idan and Hess (2013) have previously proposed, through theoretical calculations, that the colocalization and subsequent substrate channelling effect are particularly pronounced in the initial phases of the reaction, typically spanning milliseconds to seconds. They argue that while placing enzymes closely together may seem beneficial, this enhancement is mainly observed within sizable compartments like mammalian cells or the extracellular environment of the cellulosome, and it is transient (Idan and Hess 2013). Therefore, it is expected that at relatively high enzyme concentrations, the significance of the colocalization effect diminishes as the last enzyme operates as the rate-limiting factor in this study. This is due to the accumulation of product molecules of enzyme 1, which act as the substrate for enzyme 2 in the reaction. However, we hypothesise a different result if a highly active enzyme (enzyme 2) is positioned immediately following the rate-limiting enzyme (enzyme 1). When these enzymes are in close proximity, we assume that the intermediate produced by the first enzyme can be rapidly processed by the second enzyme, preventing its escape via diffusion. Proximity effects by colocalization may thus also depend on the balance of the production rates of the different enzymes. You et al. (2012) constructed a multi-enzyme complex composed of triosephosphate isomerase (TIM), aldolase (ALD) and fructose 1,6-bisphosphatase (FBP). The synthetic three-enzyme complex was assembled in vitro and had a catalytic efficiency

(k_{cat}/K_m) about 33-fold higher than the free enzyme mixture. Examining the scaffolded enzyme complex constructed by You and colleagues reveals that in that case, the second enzyme (ALD) catalysed the rate-limiting step. It is possible that the molecules produced by ALD could be converted relatively quickly by the third enzyme. When the third enzyme is in close proximity to ALD, the enzyme is not dependent on the diffusion rate of the product, as such possibly giving an advantage to the multi-enzyme complex over the free-floating FBP (You et al. 2012). However, this hypothesis does not agree with the findings of Chado et al. (2016), who investigated the effect of spatial arrangement on the activity of cascade reactions on scaffolds using kinetic Monte Carlo simulations. Their findings imply that organising enzyme placement at small length scales (i.e., below 10 nm) and in environments with high enzyme densities offers minimal advantages over random immobilisation. The authors found that even in the case of a first enzyme with a turnover rate many orders of magnitude slower than that of the second enzyme, the spatial arrangement has only a minimal impact on cascade activity (Chado et al. 2016).

Clearly, there is a significant need for improved insights on this matter. Optimising an enzyme cascade thus requires a deep understanding of the reaction mechanisms and kinetics. A detailed study of the kinetics of the separately bound docking enzymes and an accurate analysis of the intermediates released during the assay would yield further insights on the colocalization effect on each pathway enzyme present in the multi-enzyme complex. Afterwards, the complex could be subjected to another round of optimisation. Furthermore, additional research is needed to fully understand the effects of pathway enzyme colocalization in vitro environments and the requirements under which scaffolding can have a stimulating effect.

5 | Conclusions

We conclude that the first three *E. coli* glycolytic enzymes can be converted to the docking enzyme mode and subsequently scaffolded. Increasing the copy number of the rate-limiting enzyme increases the product rate. In this scenario, we demonstrate that lower enzyme densities result in higher product yields most plausibly due to the proximity effects facilitated by scaffolding, as opposed to free docking enzymes. The VersaTile DNA assembly technique is dedicated to performing optimization studies of modular proteins and complexes thereof, enabling the analysis of a larger design space through eliminating technical time-consuming hurdles in the preparatory work. This approach can be expanded to other scaffolded pathway enzymes to further investigate how the kinetics of the individual enzymes affect the outcome.

Author Contributions

Marte Elias: conceptualization, formal analysis, investigation, project administration, visualization, writing – original draft, writing – review and editing. **Kenan Meert:** conceptualization, formal analysis, investigation, data curation, writing – original draft, writing – review and editing, visualization. **Julie Vanderstraeten:** conceptualization,

investigation, supervision, writing – original draft, writing – review and editing. **Babette Lamote:** writing – review and editing. **Yves Briers:** writing – review and editing, conceptualization, funding acquisition, supervision.

Acknowledgements

The first authors hold a FWO-SB PhD grant from Research Foundation—Flanders (FWO) (1S20622N and 1S20624N), and 1SE2623N or a Baekeland grant from Flanders Innovation and Entrepreneurship (HBC.2023.0138). The authors acknowledge Universiteit Gent, Bijzonder Onderzoeksfonds UGent (BOF16/STA/024 and BOF17/DOC/086).

Conflicts of Interest

The authors declare no conflicts of interest.

Data Availability Statement

All data generated or analysed during this study are included in this published article and its [Supporting Information](#) files.

References

- Abernathy, M. H., L. He, and Y. J. Tang. 2017. “Channeling in Native Microbial Pathways: Implications and Challenges for Metabolic Engineering.” *Biotechnology Advances* 35, no. 6: 805–814. <https://doi.org/10.1016/j.biotechadv.2017.06.004>.
- Abernathy, M. H., Y. Zhang, W. D. Hollinshead, et al. 2019. “Comparative Studies of Glycolytic Pathways and Channeling Under In Vitro and In Vivo Modes.” *AICHE Journal* 65, no. 2: 483–490. <https://doi.org/10.1002/aic.16367>.
- Araiza-Olivera, D., N. Chiquete-Felix, M. Rosas-Lemus, et al. 2013. “A Glycolytic Metabolite in *Saccharomyces cerevisiae* Is Stabilized by F-Actin.” *FEBS Journal* 280, no. 16: 3887–3905. <https://doi.org/10.1111/febs.12387>.
- Bauler, P., G. Huber, T. Leyh, and J. A. McCammon. 2010. “Channeling by Proximity: The Catalytic Advantages of Active Site Colocalization Using Brownian Dynamics.” *Journal of Physical Chemistry Letters* 1, no. 9: 1332–1335. <https://doi.org/10.1021/jz1002007>.
- Bayer, E., R. Lamed, B. White, and H. Flint. 2008. “From Cellulosomes to Cellulosomics.” *Chemical Record* 8, no. 6: 364–377. <https://doi.org/10.1002/tcr.20160>.
- Bayer, E. A., P. M. Coutinho, and B. Henrissat. 1999. “Cellulosome-Like Sequences in *Archaeoglobus fulgidus*: An Enigmatic Vestige of Cohesin and Dockerin Domains.” *FEBS Letters* 463, no. 3: 277–280. [https://doi.org/10.1016/S0014-5793\(99\)01634-8](https://doi.org/10.1016/S0014-5793(99)01634-8).
- Bell, E. L., W. Finnigan, S. P. France, et al. 2021. “Biocatalysis.” *Nature Reviews Methods Primers* 1, no. 1: 46. <https://doi.org/10.1038/s43586-021-00044-z>.
- Castellana, M., M. Z. Wilson, Y. Xu, et al. 2014. “Enzyme Clustering Accelerates Processing of Intermediates Through Metabolic Channeling.” *Nature Biotechnology* 32, no. 10: 1011–1018. <https://doi.org/10.1038/nbt.3018>.
- Chado, G. R., M. P. Stoykovich, and J. L. Kaar. 2016. “Role of Dimension and Spatial Arrangement on the Activity of Biocatalytic Cascade Reactions on Scaffolds.” *ACS Catalysis* 6, no. 8: 5161–5169. <https://doi.org/10.1021/acscatal.6b01302>.
- Chen, X., J. L. Zaro, and W.-C. Shen. 2013. “Fusion Protein Linkers: Property, Design and Functionality.” *Advanced Drug Delivery Reviews* 65, no. 10: 1357–1369. <https://doi.org/10.1016/j.addr.2012.09.039>.
- Cooper, G. M. 2000. *The Cell: A Molecular Approach*. 2nd ed. Sinauer Associates.
- Deng, M.-D., D. K. Severson, A. D. Grund, et al. 2005. “Metabolic Engineering of *Escherichia coli* for Industrial Production of Glucosamine and *N*-Acetylglucosamine.” *Metabolic Engineering* 7, no. 3: 201–214. <https://doi.org/10.1016/j.ymben.2005.02.001>.
- Ding, S., E. Bayer, D. Steiner, Y. Shoham, and R. Lamed. 1999. “A Novel Cellulosomal Scaffoldin From *Acetivibrio cellulolyticus* That Contains a Family 9 Glycosyl Hydrolase.” *Journal of Bacteriology* 181: 6720–6729.
- Dueber, J. E., G. C. Wu, G. R. Malmirchegini, et al. 2009. “Synthetic Protein Scaffolds Provide Modular Control Over Metabolic Flux.” *Nature Biotechnology* 27, no. 8: 753–759. <https://doi.org/10.1038/nbt.1557>.
- Gerstmans, H., D. Grimon, D. Gutierrez, et al. 2020. “A VersaTile-Driven Platform for Rapid Hit-To-Lead Development of Engineered Lysins.” *Science Advances* 6, no. 23: eaaz1136. <https://doi.org/10.1126/sciadv.aaz1136>.
- Giegé, P., J. L. Heazlewood, U. Roessner-Tunali, et al. 2003. “Enzymes of Glycolysis Are Functionally Associated With the Mitochondrion in *Arabidopsis* Cells.” *Plant Cell* 15, no. 9: 2140–2151. <https://doi.org/10.1105/tpc.012500>.
- Guitart Font, E., and G. A. Sprenger. 2020. “Opening a Novel Biosynthetic Pathway to Dihydroxyacetone and Glycerol in *Escherichia coli* Mutants Through Expression of a Gene Variant (fsaAA129S) for Fructose 6-Phosphate Aldolase.” *International Journal of Molecular Sciences* 21, no. 24: 9625. <https://doi.org/10.3390/ijms21249625>.
- Haanstra, J. R., B. M. Bakker, and P. A. M. Michels. 2014. “In or Out? On the Tightness of Glycosomal Compartmentalization of Metabolites and Enzymes in *Trypanosoma brucei*.” *Molecular and Biochemical Parasitology* 198, no. 1: 18–28. <https://doi.org/10.1016/j.molbiopara.2014.11.004>.
- He, F. 2011. “*E. coli* Genomic DNA Extraction.” *Bio-Protocol* 1, no. 14: e97. <https://doi.org/10.21769/BioProtoc.97>.
- Idan, O., and H. Hess. 2013. “Origins of Activity Enhancement in Enzyme Cascades on Scaffolds.” *ACS Nano* 7, no. 10: 8658–8665. <https://doi.org/10.1021/nn402823k>.
- Itoh, A., Y. Ohashi, T. Soga, H. Mori, T. Nishioka, and M. Tomita. 2004. “Application of Capillary Electrophoresis-Mass Spectrometry to Synthetic In Vitro Glycolysis Studies.” *Electrophoresis* 25, no. 13: 1996–2002. <https://doi.org/10.1002/elps.200305905>.
- Jain, V. K., C. J. Y. Tear, and C. Y. Lim. 2016. “Dihydroxyacetone Production in an Engineered *Escherichia coli* Through Expression of *Corynebacterium glutamicum* Dihydroxyacetone Phosphate Dephosphorylase.” *Enzyme and Microbial Technology* 86: 39–44. <https://doi.org/10.1016/j.enzmictec.2016.01.015>.
- Jang, S., J. C. Nelson, E. G. Bend, et al. 2016. “Glycolytic Enzymes Localize to Synapses Under Energy Stress to Support Synaptic Function.” *Neuron* 90, no. 2: 278–291. <https://doi.org/10.1016/j.neuron.2016.03.011>.
- Jeong, J., S. Fushinobu, S. Ito, B. Jeon, H. Shoun, and T. Wakagi. 2003. “Characterization of the Cupin-Type Phosphoglucose Isomerase From the Hyperthermophilic Archaeon *Thermococcus litoralis*.” *FEBS Letters* 535: 200–204. [https://doi.org/10.1016/S0014-5793\(02\)03900-5](https://doi.org/10.1016/S0014-5793(02)03900-5).
- Jojima, T., and M. Inui. 2015. “Engineering the Glycolytic Pathway: A Potential Approach for Improvement of Biocatalyst Performance.” *Bioengineered* 6, no. 6: 328–334. <https://doi.org/10.1080/21655979.2015.1111493>.
- Kahn, A., S. Morais, A. P. Galanopoulou, et al. 2019. “Creation of a Functional Hyperthermostable Designer Cellulosome.” *Biotechnology for Biofuels* 12, no. 1: 44. <https://doi.org/10.1186/s13068-019-1386-y>.
- Kotlarz, D., and H. Buc. 1982. “Phosphofructokinases From *Escherichia coli*.” *Methods in Enzymology* 90: 60–70. [https://doi.org/10.1016/S0076-6879\(82\)90107-0](https://doi.org/10.1016/S0076-6879(82)90107-0).
- Lamed, R., E. Setter, R. Kenig, and E. Bayer. 1983. “The Cellulosome—A Discrete Cell-Surface Organelle of *Clostridium thermocellum* Which

- Exhibits Separate Antigenic, Cellulose-Binding and Various Cellulolytic Activities." *Biotechnology and Bioengineering* 13: 163–181.
- Lamote, B., M. da Fonseca, J. Vanderstraeten, K. Meert, M. Elias, and Y. Briers. 2023. "Current Challenges in Designer Cellulosome Engineering." *Applied Microbiology and Biotechnology* 107, no. 9: 2755–2770. <https://doi.org/10.1007/s00253-023-12474-8>.
- Ledesma-Fernandez, A., S. Velasco-Lozano, J. Santiago-Arcos, F. López-Gallego, and A. L. Cortajarena. 2023. "Engineered Repeat Proteins as Scaffolds to Assemble Multi-Enzyme Systems for Efficient Cell-Free Biosynthesis." *Nature Communications* 14, no. 1: 2587. <https://doi.org/10.1038/s41467-023-38304-z>.
- Li, H., H. Su, S. B. Kim, et al. 2012. "Enhanced Production of Trehalose in *Escherichia coli* by Homologous Expression of otsBA in the Presence of the Trehalase Inhibitor, Validamycin A, at High Osmolarity." *Journal of Bioscience and Bioengineering* 113, no. 2: 224–232. <https://doi.org/10.1016/j.jbiosc.2011.09.018>.
- Mesojednik, S., and M. Legiša. 2005. "Posttranslational Modification of 6-Phosphofructo-1-Kinase in *Aspergillus niger*." *Applied and Environmental Microbiology* 71, no. 3: 1425–1432. <https://doi.org/10.1128/aem.71.3.1425-1432.2005>.
- Moon, T. S., S.-H. Yoon, A. M. Lanza, J. D. Roy-Mayhew, and K. L. J. Prather. 2009. "Production of Glucaric Acid From a Synthetic Pathway in Recombinant *Escherichia coli*." *Applied and Environmental Microbiology* 75, no. 3: 589–595. <https://doi.org/10.1128/aem.00973-08>.
- Nelson, D. L., and M. M. Cox. 2013. *Lehninger Principles of Biochemistry*. 6th ed. W. H. Freeman and Company.
- Roberts, A. D., K. A. P. Payne, S. Cosgrove, et al. 2021. "Enzyme Immobilisation on Wood-Derived Cellulose Scaffolds via Carbohydrate-Binding Module Fusion Constructs." *Green Chemistry* 23, no. 13: 4716–4732. <https://doi.org/10.1039/d1gc01008e>.
- Stevenson, B. J., J. W. Liu, P. W. Kuchel, and D. L. Ollis. 2012. "Fermentative Glycolysis With Purified *Escherichia coli* Enzymes for In Vitro ATP Production and Evaluating an Engineered Enzyme." *Journal of Biotechnology* 157, no. 1: 113–123. <https://doi.org/10.1016/j.jbiotec.2011.09.019>.
- Studier, F. 2005. "Protein Production by Auto-Induction in High-Density Shaking Cultures." *Protein Expression and Purification* 41: 207–234. <https://doi.org/10.1016/j.pep.2005.01.016>.
- Sze, J. H., J. C. Brownlie, and C. A. Love. 2016. "Biotechnological Production of Hyaluronic Acid: A Mini Review." *3 Biotech* 6, no. 1: 67. <https://doi.org/10.1007/s13205-016-0379-9>.
- Ullah, M. W., W. A. Khattak, M. Ul-Islam, S. Khan, and J. K. Park. 2016. "Metabolic Engineering of Synthetic Cell-Free Systems: Strategies and Applications." *Biochemical Engineering Journal* 105: 391–405. <https://doi.org/10.1016/j.bej.2015.10.023>.
- Vanderstraeten, J., and Y. Briers. 2020. "Synthetic Protein Scaffolds for the Colocalisation of Co-Acting Enzymes." *Biotechnology Advances* 44, no. 23: 107627. <https://doi.org/10.1016/j.biotechadv.2020.107627>.
- Vanderstraeten, J., M. J. M. Da Fonseca, P. De Groote, et al. 2022a. "Combinatorial Assembly and Optimisation of Designer Cellulosomes: A Galactomannan Case Study." *Biotechnology for Biofuels and Bioproducts* 15, no. 1: 60. <https://doi.org/10.1186/s13068-022-02158-2>.
- Vanderstraeten, J., B. Lamote, M. J. M. Da Fonseca, P. De Groote, and Y. Briers. 2022b. "Conversion of the Free *Cellvibrio japonicus* Xyloglucan Degradation System to the Cellulosomal Mode." *Applied Microbiology and Biotechnology* 106, no. 17: 5495–5509. <https://doi.org/10.1007/s00253-022-12072-0>.
- Vazana, Y., Y. Barak, T. Unger, et al. 2013. "A Synthetic Biology Approach for Evaluating the Functional Contribution of Designer Cellulosome Components to Deconstruction of Cellulosic Substrates." *Biotechnology for Biofuels* 6, no. 1: 182. <https://doi.org/10.1186/1754-6834-6-182>.
- Vazana, Y., S. Morais, Y. Barak, R. Lamed, and E. Bayer. 2012. "Designer Cellulosomes for Enhanced Hydrolysis of Cellulosic Substrates." *Methods in Enzymology* 510: 429–452. <https://doi.org/10.1016/B978-0-12-415931-0.00023-9>.
- Vazquez-Gonzalez, M., C. Wang, and I. Willner. 2020. "Biocatalytic Cascades Operating on Macromolecular Scaffolds and in Confined Environments." *Nature Catalysis* 3, no. 3: 256–273. <https://doi.org/10.1038/s41929-020-0433-1>.
- Wang, J., and Y. Yan. 2018. "Glycolysis and Its Metabolic Engineering Applications." In *Engineering Microbial Metabolism for Chemical Synthesis*, 1–33. World Scientific Publishing Europe Ltd. https://doi.org/10.1142/9781786344304_0001.
- Yong, Y., P. Ouyang, J. Wu, and Z. Liu. 2020. "A Diffusion-Reaction Model for One-Pot Synthesis of Chemicals With Enzyme Cascades." *ChemCatChem* 12, no. 2: 528–535. <https://doi.org/10.1002/cctc.201901161>.
- Yoon, S., M.-J. Han, H. Jeong, et al. 2012. "Comparative Multi-Omics Systems Analysis of *Escherichia coli* Strains B and K-12." *Genome Biology* 13, no. 5: R37. <https://doi.org/10.1186/gb-2012-13-5-r37>.
- You, C., S. Myung, and Y. H. P. Zhang. 2012. "Facilitated Substrate Channeling in a Self-Assembled Trifunctional Enzyme Complex." *Angewandte Chemie International Edition* 51, no. 35: 8787–8790. <https://doi.org/10.1002/anie.201202441>.
- Zhang, Y. 2011. "Substrate Channeling and Enzyme Complexes for Biotechnological Applications." *Biotechnology Advances* 29: 715–725. <https://doi.org/10.1016/j.biotechadv.2011.05.020>.
- Zheng, R. L., and R. G. Kemp. 1992. "The Mechanism of ATP Inhibition of Wild Type and Mutant Phosphofructo-1-Kinase From *Escherichia coli*." *Journal of Biological Chemistry* 267, no. 33: 23640–23645. [https://doi.org/10.1016/S0021-9258\(18\)35886-1](https://doi.org/10.1016/S0021-9258(18)35886-1).

Supporting Information

Additional supporting information can be found online in the Supporting Information section.